Release of HIV-1 particles from the viral compartment in macrophages requires an associated cytoskeleton and is driven by mechanical constraints

Vasco Rodrigues[1], Sarah Taheraly[1], Mathieu Maurin[1], Mabel San-Roman[2], Emma Granier[1], Anaël Hanouna[1], Phillippe Benaroch[1]

1- Institut Curie, PSL Research University, INSERM U932, Paris, France
2- Institut Curie, UMR3215, Paris, France

Address correspondence to:

Vasco Rodrigues – vteixeir@curie.fr

Philippe Benaroch - Philippe.Benaroch@curie.fr

Abstract

A defining feature of HIV-1 replication in macrophages is that viral assembly occurs at the limiting membrane of a compartment often named VCC (virus-containing compartments) that is connected to the extracellular medium. The newly formed viral progeny pinches of the membrane and accumulates in the lumen of the VCC. While HIV budding has been extensively studied, very little is known about how viral particles present in the lumen of VCC are released in the extracellular medium. Here we show that the actin dynamics are critical for this process by combining ultrastructural analyses, time-lapse microscopy and perturbations of the actin cytoskeleton. We found that jasplakinolide, which stabilizes actin fibres, inhibited viral release from HIV-1-infected macrophages, but not from infected HeLa cells. Furthermore, in jasplakinolide-treated macrophages, VCC became scattered and no longer co-localized with the integrin CD18, nor the phosphorylated form of the focal adhesion kinase PYK2. Inhibition of PYK2 activity in infected macrophages promoted intracellular retention of viral particles in VCC that were no longer connected to the plasma membrane. Finally, we stimulated the rapid release of viral particles from the VCC by subjecting infected macrophages to frustrated phagocytosis. As macrophages spread on IgG-coated glass surfaces, VCC rapidly migrated to the basal membrane and released their viral content in the extracellular medium, which required their association with CD18 and the actin cytoskeleton. These results highlight that VCC trafficking and virus release are intimately linked to the reorganization of the macrophage actin cytoskeleton in response to external physical cues, suggesting that it might be regulated in tissues by the mechanical stress to which these cells are exposed.

35 **Introduction**

36 Macrophages are embedded in many tissues where they ensure specific functions. Early studies
37 established that HIV-1-infected patients possess infected macrophages in many of their tissues
38 (Orenstein et al., 1988). Usage of monocyte-derived macrophages (MDM) exposed to HIV-1 *in vitro*
39 allowed the study of the viral replication cycle and revealed some of its specific features as compared
40 to how it replicated in T lymphocytes (Rodrigues et al., 2017; Sattentau and Stevenson, 2016). Viral
41 assembly takes place in macrophages at the limiting membrane of a compartment that appears
42 intracellular. The newly formed virions, pinch off from this membrane in the lumen of the
43 compartment, hence called VCC for virus-containing compartments, where they accumulate.
44 Interestingly, compartments with very similar characteristics are also present in uninfected
45 macrophages, as they similarly express tetraspanins (CD9, CD81 and CD63) (Deneka et al., 2007), and
46 the scavenger receptor CD36 (Berre et al., 2013). Upon HIV-1 infection, newly synthesized Gag is
47 recruited to these pre-existing compartments that become *de facto* VCC (Berre *et al.*, 2013).

48 The VCC possess a very intricate architecture and are often connected to the extracellular medium by
49 channels or conduits that are too narrow to allow the virions to exit but that permit fluid exchanges
50 (Gaudin et al., 2013; Welsch et al., 2007). They remain mostly inaccessible to macromolecules
51 delivered from the extracellular media, such as antibodies (Chu et al., 2012). The precise nature of
52 the VCC has been debated but the current view holds that it originates from tetraspanin-rich zones of
53 the plasma membrane that have been internally sequestered. While VCC are generally considered as
54 continuous with the plasma membrane, recent work also evidenced the presence of completely
55 enclosed compartments that could fuse with plasma membrane-connected compartments (Ladinsky
56 et al., 2019). These studies highlight a rather complex and dynamic structure that results in a more
57 complex release of viral particles as compared with other cell types.

58 How the virions stocked in the VCC lumen are released in the extracellular medium remains an open
59 question. To our knowledge, a single study reported that the release of viral particles from the VCC
60 can be induced. Exposure of an infected MDM to extracellular ATP (eATP) prompted a rapid discharge
61 of the viral particles stored in the VCC, via stimulation of the P2X7 purinergic receptor (Graziano et al.,
62 2015). The rapid and drastic remodelling of the cell shape and actin cytoskeleton that eATP induces
63 on HIV-infected MDMs may underlie its impact on viral release. This interpretation raises the question
64 of how the structure of the VCC, their trafficking, and consequently viral particle release are impacted
65 by or depend on the actin cytoskeleton.

66 The VCC are surrounded by a meshwork of filamentous actin tightly associated with its external
67 membrane (Mlcochova et al., 2013; Pelchen-Matthews et al., 2012), which is often decorated by an

68 electron dense molecular coat that appears to anchor the actin cytoskeleton to the compartment
69 (Pelchen-Matthews *et al.*, 2012). These coats have striking resemblances with focal adhesions, as they
70 contain the ß2-integrin CD18 and its associated CD11b and CD11c α-integrins. Focal adhesion linker
71 proteins, such as talin, vinculin and paxillin are also found at these molecular coats (Pelchen-Matthews
72 *et al.*, 2012). Silencing CD18 in HIV-1 infected macrophages, did not alter viral release over a 24-hour
73 window. Whether a longer period of analysis impacts viral release was not assessed; nevertheless,
74 CD18 silencing led to scattering of the VCC across the cell (Pelchen-Matthews *et al.*, 2012), suggesting
75 that these coats are an integral part of the compartment.

76 In macrophages, many focal adhesion-mediated processes such as cell migration are regulated by
77 Focal Adhesion Kinase (FAK)-related proline-rich tyrosine kinase 2 (PYK2) (Okigaki et al., 2003). PYK2
78 promotes the assembly of focal adhesions at the leading edge, and their disassembly at the trailing
79 edge to ensure net forward movement (Zhu et al., 2018). The full breadth of PYK2 activators and
80 substrates remain incompletely understood, but it is generally considered to act at the cross-roads
81 between integrin and small GTPases, such as Rho (Schaller, 2010).

82 It remains unclear how the VCC structure and HIV particle release are impacted by these focal
83 adhesion-like coats and PYK2 signalling and, in general, our understanding on how the actin
84 cytoskeleton impacts HIV release from macrophages remains rudimentary. We report here that
85 pharmacological stabilization of actin fibres led to scattering of the VCC and impeded viral particle
86 release from infected MDM. This was paralleled by decreased association of the integrin CD18 and of
87 the phosphorylated form of the kinase PYK2 with the compartment. Specific inhibition of PYK2 led to
88 accumulation of viral particles in VCC that lost connection to the plasma membrane. Finally, subjecting
89 infected MDM to frustrated phagocytosis on glass coverslip induced rapid trafficking of VCC to the
90 surface and viral release. Such trafficking required the compartment to be associated with CD18 and
91 the actin cytoskeleton. We propose that focal adhesion-like coats are regulated by PYK2 and anchor
92 the actin cytoskeleton to the VCC to promote HIV release from macrophages.

93 **Results**

94 **1. Actin dynamics modulates viral particle release from HIV-1-infected macrophages**

95 In MDMs infected with HIV-1-GAG-iGFP-ΔENV-VSVG for 4 days, phalloidin staining can be readily
96 observed around the VCC, confirming previous observations (Mlcochova *et al.*, 2013) (Fig. 1A-B). F-
97 Actin appears docked at or surrounding the compartment, rather than in its lumen (see 3D inset in
98 Fig. 1B). Ultrastructural analysis by electron microscopy (EM) revealed the presence of actin filaments
99 anchored at and radiating from the VCC (Fig. S1A-B). Live imaging of MDMs transduced with Lifeact-
100 mCherry and infected with HIV-1-GAG-iGFP-ΔEnv-VSVG confirmed that the VCC and the actin
101 cytoskeleton are in proximity to each other, and exhibit synchronized movements (Fig. 1C and Video
102 S1).

103 To explore how the actin cytoskeleton may impact on the structure of the VCC and viral release, we
104 first employed a cell micropatterning technique to physically manipulate the actin cytoskeleton
105 organization in HIV-1-infected MDMs (Fig. S2A-S2B). Indeed, adherent cells adapt to the micropattern
106 shape by remodelling their actin cytoskeleton as to maximize adhesion (Thery, 2010). We observed
107 that plating HIV-1-infected MDMs on distinct micropatterns impacted on the total volume of the VCC
108 (Fig. S2A-S2B). This was particularly evident in crossbow-shaped macrophages, which presented stress
109 fibres at the non-adherent edges, and bore significantly smaller VCCs (Fig. S2A-S2B). Nonetheless,
110 these cells did not remain immobile over the patterned areas for prolonged periods of time,
111 precluding any accurate analysis on viral particle release. We turned thus into pharmacological
112 manipulation of the actin cytoskeleton of infected macrophages to ascertain how it impacts on the
113 VCC size and structure as well as viral release.

114 We infected MDMs with HIV-1-ΔENV-VSVG for 4 days to allow formation of VCCs and treated them
115 with a panel of pharmacological modulators of the actin cytoskeleton. Over the next 24 hours, we
116 observed that the F-actin stabilizing drug, jasplakinolide, reduced the release of viral particles (Fig.
117 1D), as measured by our in-house CBA assay that specifically detects the HIV-1 p24 capsid protein (Fig.
118 S3A). None of the other cytoskeleton-modifying drugs had significant effects on viral release over the
119 24 hours period (Fig. 1D). Jasplakinolide was also the sole drug to induce retention of p24 inside the
120 macrophage during the 24 hours treatment period, suggesting that the viral particles are retained
121 inside the cell, hence their decreased concentration in the supernatant (Fig. 1E-G). Interestingly,
122 treatment of HIV-1-infected HeLa cells with the same cytoskeleton modulators failed to induce any
123 significant changes in p24 release over vehicle-treated cells (Fig. S3B), suggesting that the effect of
124 jasplakinolide treatment implicates the VCC, a macrophage-specific structure.

125

126 **2. Stabilization of actin fibres impacts VCC structure and architecture**

127 We next asked how jasplakinolide treatment results in retention of p24 in the macrophage, by
128 examining its impact on the VCC by confocal microscopy. MDMs were infected with HIV-1-GAG-iGFP-
129 ΔENV-VSVG for 4 days, treated or not with a non-toxic dose of jasplakinolide for 24 hours and analysed
130 by confocal microscopy. As expected, the drug had a strong impact on the general macrophage
131 morphology, as cells rounded up and lost their typical spreading over the substrate (Fig. 2A). While
132 this led to significant decrease in cell volume (Fig. 2B), treatment with jasplakinolide increased the
133 total volume of the VCC (Fig. 2C-D). The average intensity of the Gag-iGFP signal was similar between
134 treated and not treated cells (Fig. 2E), although the compartment spread more evenly throughout the
135 cell (Fig. 2F), suggesting a loss in its compactness. These observations were confirmed by EM, as the
136 typical VCC in vehicle-treated cells appear to fragment into smaller, but more numerous,
137 compartments after treatment with jasplakinolide (Fig. 2G). Jasplakinolide-treated MDMs also
138 exhibited massive accumulations of F-actin that occupied large sections of the cytoplasm (Fig. 2G,
139 bottom left panel). Their appearance is concomitant with loss of the actin filaments that typically
140 radiate from the VCC in control macrophages. Overall, these data suggest that drug-induced F-actin
141 stabilization leads to loss of the organized actin filaments that are anchored at the VCC.
142 Consequentially, compartments become dispersed throughout the cell and accumulate, resulting in
143 impaired viral release.

144

145 **3. Stabilization of actin fibres relocalizes the integrin CD18 away from the VCC-limiting membrane**

146 Previous work reported that the β2-integrin CD18 is present in focal adhesion-like electron dense
147 regions at the limiting membrane of the VCC and is critical for the integrity of the VCC (Pelchen-
148 Matthews *et al.*, 2012). We confirmed the presence of electron dense regions that coat the VCC and
149 that serve as anchoring sites for the actin cytoskeleton (Fig. 3A, Fig. 2G and Fig. S1A-B). These coats
150 were also present in VCCs at, or close to, the cell surface (Fig. 3B), suggesting their implication on the
151 trafficking of the compartment. Confocal immunofluorescence confirmed that CD18 surrounds the
152 VCC (Fig. 3C-D). However, treatment with jasplakinolide lead to a significant decrease on the
153 enrichment of CD18 at the vicinity of the VCC (Fig. 3C-D). Analysis by EM confirmed that the electron
154 dense coats typical of control MDMs, were no longer observable in the smaller and more numerous
155 VCCs of jasplakinolide-treated cells (Fig. 3E-F and Fig 2G). Our data indicates that pharmacological
156 stabilization of actin leads VCC to lose their association focal adhesion-like coats and the integrin CD18,
157 which possibly underlies the accumulation of viral particles inside the cell.

158

159 **4. The phosphorylated form of the focal adhesion kinase PYK2 localizes at the VCC**

160 Because of the similarities between focal adhesions and the electron dense coats around the VCC, we
161 evaluated whether PYK2, a non-receptor tyrosine FAK that governs the focal adhesion response to
162 integrin-mediated signalling, plays a role on the VCC structure and HIV-1 release from macrophages.
163 A 4-day infection of MDMs with HIV-1-ΔENV-VSVG led to activation of PYK2, as evidenced by an
164 increase in the levels of phosphorylated PYK2 at Tyr402 (Fig. 4A), in agreement with a previous report
165 (Del Corno et al., 2001). Confocal microscopy revealed that P-PYK2 (Y402) localized mostly to the basal
166 surface of the macrophage and was organized into large clusters that likely corresponded to
167 podosomes (Fig. 4C). Yet, a small pool of P-PYK2 located at the VCC in DMSO-treated cells (Fig. 4C).
168 While jasplakinolide treatment had no effect on the global levels of PYK2 Tyr 402-phosphorylation
169 induced by HIV-1 infection (Fig. 4A), it led to loss of the enrichment of P-PYK2 at the VCC observed in
170 vehicle-treated cells, as the P-PYK2 signal dispersed evenly throughout the cell (Fig. 4B-C). These data
171 indicates that jasplakinolide treatment induces loss of association of the phosphorylated form of PYK2
172 from the VCC, accompanying the loss of CD18 and focal adhesion-like coats.

173

174 **5. Active PYK2 participates in viral particle release from the VCC**

175 Overall, our results hint at a possible role for PYK2 as coordinating actin dynamics at the VCC, since (1)
176 its active phosphorylated form localizes to the compartment, and (2) jasplakinolide treatment disrupts
177 its localization at the VCC, concomitant with loss of the electron dense regions and CD18 expression
178 at the compartment. To directly test this hypothesis, we treated HIV-1-ΔENV-infected MDMs with
179 PF431396 (PF396), a dual FAK/PYK2 inhibitor that has higher affinity for PYK2 over FAK (IC50 values of
180 2 and 11 nM, respectively). PF396 prevented the phosphorylation of PYK2 induced by HIV-1 infection
181 and decreased p24 release from infected macrophages, over a 96-hour period and, conversely,
182 promoted its retention inside the cell (Fig. 5A-C). We next examined the VCCs of macrophages infected
183 with HIV-1 GAG-iGFP-ΔENV-VSVG for 4 days and treated for additional 4 days with PF396 (Fig. 5D).
184 While PF396 had no evident impact on the macrophage morphology, including cell volume (Fig 5E), it
185 led to a significant increase in the compartment volume (Fig. 5F), without an impact on the mean
186 intensity of the Gag-iGFP signal (Fig. 5G). These VCC from PF396-treated MDMs often had a granular
187 or reticulated appearance (Fig. 5D and S4A). While F-actin remained localized close to the
188 compartment in PF396-treated cells, it appeared evenly distributed throughout the VCC, rather than
189 being concentrated as patches in one side, as commonly observed in vehicle-treated cells (Fig 5D).
190 Despite their larger volume, VCC from PF396 treated cells were more compact, as revealed by their
191 decreased spreading scores (Fig 5H). The VCCs from PF396-treated cells also frequently had a

192 perinuclear location (Fig. 5D, 5K and Fig. S4A), although the average distance of the VCC to the nuclear
193 centroid did not reach statistical significance (Fig. 5I). Finally, while CD18 remained enriched in the
194 vicinity of the VCC after PF396 treatment, its distribution was more even, as observed with F-actin
195 (Fig. 5J and Fig. S4A).

196 Due to the increased compactness and perinuclear accumulation of VCC from PF396-treated
197 macrophages, we hypothesized that the VCC continuity with the plasma membrane may be altered
198 after exposure to the drug, which could explain the decreased viral particle release. We thus exposed
199 PF396-treated or vehicle-treated macrophages to CellBrite®, a non-permeable lipophilic dye that can
200 withstand fixation. Strikingly, we observed strong accumulation of the dye in VCC from DMSO-treated
201 macrophages, while those from PF396-treated cells were generally negative for CellBrite staining (Fig.
202 5K-M and Fig. S5A). Finally, PF396 treatment did not render VCC accessible to an anti-CD44 antibody
203 added from the extracellular media (Fig. S6A), although VCC from PF396-treated cells could still be
204 stained with anti-CD44 after cell permeabilization (Fig. S6B). PYK2 is known for its critical role in
205 regulating actin dynamics at focal adhesions (Schaller, 2010). Our data suggest that it is endowed with
206 a similar role at the VCC, promoting its trafficking to the surface and regulating its connectivity to the
207 plasma membrane.

208

209 **6. Frustrated phagocytosis of HIV-1-infected MDM induces the rapid release of viral particles from**
210 **VCC**

211 While our previous experiments have examined the role of the actin cytoskeleton in regulating HIV
212 release from resting macrophages, we aimed to observe its impact in cells undergoing a dynamic
213 process. For that, we subjected HIV-1-infected MDMs to frustrated phagocytosis. In this experimental
214 system, macrophages spread rapidly on the substrate, driven by actin polymerization that promotes
215 a fast and concentric extension of pseudopods, until the plasma membrane tension increases to a
216 point that no longer allows further spreading (Masters et al., 2013). If an HIV-1-infected macrophage
217 is subjected to frustrated phagocytosis, we hypothesize that VCC act as membrane reservoirs that can
218 be deployed rapidly to the surface to counteract the increase in plasma membrane tension, and that
219 their anchoring to the cytoskeleton would be required for such rapid deployment. We thus seeded
220 MDMs, infected for 3 days with HIV-1-GAG-iGFP-ΔENV-VSVG, over a human IgG-coated surface and
221 performed live imaging. As exemplified in Fig. 6A, the macrophage spread rapidly on the surface with
222 its projected area more than doubling in 20 minutes (Fig. 6A-B and Video S2). We further observed a
223 steady decrease in the volume of the VCC starting at around 8 minutes (Fig 6A and 6B). The
224 compartment appears to migrate towards the basal surface, as the cell spreads, where its intensity

225 decreases, presumably due to virion release (Fig. 6A, xz planes). Indeed, by quantifying the amount of
226 p24 in the culture supernatant, we observed a rapid release of the capsid protein from MDMs seeded
227 over IgG-coated coverslips as compared with control coverslips or control coverslips + IgG added at
228 the same time as the cells ("Soluble IgG") (Fig. 6C), during the first two hours. Such rapid kinetics
229 suggests that it is the preformed viral particles stored in VCCs that are released during frustrated
230 phagocytosis and not a general increase in viral production due to macrophage activation. Supporting
231 this idea, at later time-points there were no differences in the concentration of p24 released from
232 macrophages seeded in the three different conditions (Fig. 6C). Thus, as macrophages spread during
233 frustrated phagocytosis, VCC appear to be pulled to the basal surface of the cell, where they release
234 their contents.

235 We next tested whether the actin cytoskeleton participates in VCC trafficking during frustrated
236 phagocytosis. We fixed HIV-1-infected MDMs subjected to frustrated phagocytosis or in control
237 conditions and examined by confocal microscopy (Fig. 6D). In cells under frustrated phagocytosis, F-
238 actin concentrated on the protruding edges and as expected, these cells increased in volume (Fig. 6E).
239 The VCC, conversely, were significantly reduced in their volume in cells undergoing frustrated
240 phagocytosis (Fig. 6F), as was the mean intensity of the Gag-iGFP signal (Fig. 6G). Interestingly, the
241 remaining VCC in MDMs under frustrated phagocytosis were mostly devoid of associated F-actin (Fig.
242 6D). Furthermore, while VCC from control MDMs were associated with CD18, as expected, after
243 frustrated phagocytosis the remaining VCCs lost this association (Fig. 6H and Fig. S7A). Finally, P(Y402)-
244 PYK2 concentrated mostly in the protruding edges in cells under frustrated phagocytosis, while
245 remaining VCC in general lacked P-PYK2 (Fig. S7B). This strongly suggests that the rapid deployment
246 of the VCCs to the surface that occurs during frustrated phagocytosis, requires an associated
247 cytoskeleton and focal adhesion-like coats, and that compartments lacking such associated complexes
248 remain inside the macrophage after frustrated phagocytosis.

249

250 **Discussion**

251 Overall, our data highlights the importance of the actin cytoskeleton and associated factors in
252 regulating the release of HIV-1 from its VCC in macrophages, likely by providing a physical anchor that
253 promotes its movement, connectivity with the plasma membrane and, consequentially, viral release.
254 While previous studies addressed the presence of an actin cytoskeleton associated with the VCC, and
255 its importance for viral release, the molecular details remained unknown. Here, we uncover an
256 important role for the CD18-PYK2 axis as modulators of the VCC structure, its trafficking dynamics and
257 viral release.

258 Cell shape is governed by the actin cytoskeleton, particularly cortical actin (Chalut and Paluch, 2016).
259 To start exploring the importance of the actin cytoskeleton on HIV release from macrophages, we
260 developed a micropatterning technique for HIV-1-infected macrophages. Our data indicates that the
261 VCC's structure and size are sensitive to cell shape. Particularly, macrophage adhesion to the crossbow
262 pattern imposes strong physical constraints resulting in smaller VCC that are mostly devoid of
263 surrounding F-actin. Accurate estimation of viral particle release was not achievable due to the strong
264 adhesive properties of macrophages which tended to invade the surrounding anti-adhesive PEG-based
265 substrate after a few hours of seeding over patterns. Nevertheless, our finding that PEG-Silane can, at
266 least temporarily, efficiently micropattern primary human MDMs, may serve as a useful tool for future
267 studies employing micropatterning to study human macrophage biology.

268 By exposing infected MDMs to different pharmacologic modulators of the cytoskeleton we found that
269 the F-actin stabilizing drug jasplakinolide significantly impacted on viral release to the supernatant. A
270 previous report demonstrated an increase in viral release from HIV-1-infected macrophages after
271 treatment with the actin depolymerizing drug latrunculin, or the actin polymerization inhibitors,
272 cytochalasin E or D (Mlcochova *et al.*, 2013). In our hands, the actin depolymerizing drug mycalolide B
273 had no significant effect on viral release over a 24-hour period. Differences in the viral strains
274 employed, experimental conditions or the distinct mechanisms through which mycalolide B and
275 latrunculin depolymerize actin (Hayashi-Takanaka et al., 2019), may account for the divergent results.

276 The ARP2/3 complex inhibitor CK666 had no effect in viral release over 24 hours. Longer exposure to
277 CK666 led to toxic effects, so we cannot exclude that in the long-term actin polymerization may be
278 required for viral release. Nevertheless, at least in the short term, actin polymerization may not be
279 necessary for HIV release from macrophages. Similarly, the myosin II inhibitor blebbistatin had no
280 significant effect on viral release over a 24-hour period, suggesting that actomyosin contraction is not
281 a major driver of viral release, at the steady state.

282 The use of pharmacological manipulation of the actin cytoskeleton is not without its shortcomings,
283 due to its critical importance in multiple other biological processes. During HIV infection actin impacts
284 virtually on every step of the viral cycle (Ospina Stella and Turville, 2018). To minimize "off-target"
285 effects, we allowed the establishment of the infection and formation of VCCs for 4 days before
286 addition of the cytoskeleton modulators, as to exclude any effect on the early steps of the viral cycle.
287 Nevertheless, we can't dismiss certain unwanted effects may indirectly impact on HIV release.

288 Jasplakinolide treatment had no effect on p24 release from infected HeLa cells. Previous work showed
289 that while latrunculin augmented viral release from macrophages, it had no effect on infected HEK
290 293 cells (Mlcochova *et al.*, 2013). Given that in these cell lines HIV-1 viral particles directly bud to the
291 extracellular media, their release may not be impacted by modulating actin dynamics. Nevertheless,
292 studies addressing the impact of viral release from non-macrophage cells often yielded inconsistent
293 results (Ospina Stella and Turville, 2018). Some reports suggest that actin may be important for the
294 assembly and budding processes (Thomas et al., 2015; Wen et al., 2014), but this is at odds with a
295 study that tracked individual budding sites in real-time in HeLa cells, demonstrating that assembly and
296 budding proceed unimpaired even after total depolymerization of actin (Rahman et al., 2014). Thus,
297 it will be important to standardize experimental approaches to study the effects of the actin
298 cytoskeleton on HIV assembly and budding. In macrophages, the field will face the added challenge of
299 discriminating between the impact of actin modulation on viral assembly and budding, and its
300 influence on VCC trafficking, as both may impact on viral release.

301 In HIV-infected macrophages exposed to jasplakinolide, VCC scattered throughout the cell and were
302 smaller, but more numerous, such that their total volume increased. They were devoid of associated
303 actin, CD18 and the focal adhesion-like coats typically found in non-treated infected cells. In non-
304 treated and infected macrophages, we observed that actin bundles frequently radiated from these
305 VCC coats, suggesting that they are the site of anchoring of the cytoskeleton to the compartment.
306 Jasplakinolide induces the loss of these structures, concomitant with the fragmentation of the
307 compartment, suggesting an important role for the coats and their associated cytoskeleton in
308 maintaining the integrity of the VCC.

309 Our frustrated phagocytosis assays indicate an important role for the actin cytoskeleton and VCC-
310 associated CD18 in the trafficking of the compartment to the surface. We show that the drastic
311 remodelling of the macrophage morphology that occurs in frustrated phagocytosis leads to rapid viral
312 release, associated with loss of VCCs. Importantly, those VCC remaining in the cell after frustrated
313 phagocytosis were small and mostly devoid of actin and CD18, suggesting that these are required for
314 rapid VCC trafficking to the surface and viral release. VCC appear to be pulled rapidly to the basal
315 surface of the cell during frustrated phagocytosis. Is the pulling force transmitted through the actin

316 bundles connected to the compartment, as our observations suggest? If yes, where does such force
317 originate from, and what is the role of the electron dense coats that surround the VCC? One may
318 speculate that the coats act as traction points, upon which pulling forces may act, in a manner akin to
319 focal adhesions during mesenchymal cell migration (Bear and Haugh, 2014). In this scenario, one
320 would expect a role for actomyosin contraction at the origin of the pulling forces acting on the VCC.
321 While we failed to observe any effect of myosin II inhibition in viral release from macrophages at the
322 steady state, its impact may be more prominent during an event such as frustrated phagocytosis,
323 where VCCs rapidly traffic through the cell. However, given the known role for myosin II in the
324 formation of phagocytic cups, we could not test the impact of its inhibition in viral release during
325 frustrated phagocytosis (Olazabal et al., 2002). Future studies, employing alternative approaches able
326 to specifically isolate the role of myosin II in VCC trafficking could help answer this question.

327 We found that the phosphorylated form of the kinase PYK2 localizes at the VCC, and that jasplakinolide
328 treatment redistributes it throughout the cell. The key role this kinase plays in regulating the dynamics
329 of focal adhesions in macrophages, prompted us to explore its importance in HIV release. Inhibiting
330 PYK2 led to viral particle accumulation in the macrophage, associated with larger VCC that often had
331 a granular appearance. While F-actin and CD18 associated with the VCC via patches or focal points in
332 control cells, treatment with the PYK2 inhibitor led to a more even distribution of these factors on the
333 compartment. This suggests that PYK2 inhibition leads to altered organization of the focal adhesion-
334 like coats that attach the actin cytoskeleton to the VCC, which may possibly underlie its impact on viral
335 release. PYK2 inhibition also led VCC to lose plasma membrane connectivity, concomitant with the
336 increased compaction of the compartment and perinuclear location. In vehicle-treated and infected
337 cells, certain VCC were connected to the plasma membrane, while others not, in agreement with
338 previous observations (Deneka *et al.*, 2007; Gaudin *et al.*, 2013). In bone marrow macrophages from
339 humanized mice infected with HIV-1, completely enclosed compartments were often perceived, and
340 these occasionally fused with plasma membrane-connected compartments (Ladinsky *et al.*, 2019).
341 Integrating these observations with our new data, VCC appear to alternate between enclosed and
342 plasma membrane-connected states, in a manner regulated by PYK2 activity. These enclosed
343 compartments maintain the expression of VCC classical markers such as CD18 and CD44, despite
344 remaining inaccessible to antibodies added prior to cell fixation and permeabilization.

345 PYK2 phosphorylation has been previously reported during HIV-1 infection and occurs downstream of
346 co-receptor engagement by the envelope glycoprotein gp120 (Del Corno *et al.*, 2001), but not when
347 Δ*Env,* pseudotyped viruses are used (Davis et al., 1997). Thus, our data points to a distinct, lasting,
348 activation of PYK2 during HIV-1 infection mediated by an undescribed mechanism. In macrophages,
349 HIV can reprogram cell migration, via its accessory protein Nef, towards a mesenchymal mode

350 (Verollet et al., 2015), which depends on adhesive structures such as podosomes (Van Goethem et al.,
351 2010) and is associated with PYK2 activation (Duong and Rodan, 2000). It is thus possible that a later
352 activation of PYK2 by HIV Nef may contribute to enhancing viral release from macrophages.

353 A limitation of our study that could be explored in future research was the use of *Env*-deficient viruses
354 pseudotyped with VSV-G to achieve single-cycle infections. This strategy avoids propagation of the
355 infection, which could indirectly impact the quantification of viral release. However, in our cultures,
356 direct viral transmission from one cell to another does not occur due to the absence of the viral
357 envelope. VCC are often observed in proximity to the viral synapse that forms between an infected
358 and a target cell (Duncan et al., 2014; Gousset et al., 2008), where they potentially participate in direct
359 viral transmission. Interestingly, direct transmission of HIV-1 from macrophages to $CD4^+$ T cells is
360 inhibited by jasplakinolide (Duncan *et al.*, 2014), suggesting that the same actin-dependent
361 mechanisms that regulate VCC trafficking for viral release, also impact its redistribution towards viral
362 synapses. It would be valuable to explore whether the factors described in this work as regulating viral
363 release and VCC trafficking, such as PYK2 or the VCC coats, also play a role in cell-to-cell HIV
364 transmission.

365 To conclude, whether at the steady-state or upon a stimulus that requires sudden and drastic changes
366 in macrophage morphology, VCC appear to be dynamic structures that traffic through the cell in a
367 manner that depends on its associated actin and microtubule cytoskeleton (Gaudin et al., 2012). In
368 tissues, macrophages are constantly subjected to mechanical constraints as they navigate through
369 crowded tissues, in a manner dependent on cytoskeletal dynamics. Our work suggests that HIV may
370 exploit the macrophage biology to promote its own release and propagation.

371 **Material and Methods**

372

373 Cells

374 Plasmapheresis residues from healthy adult donors were obtained from the Établissement Français
375 du Sang (Paris, France). All donors signed informed consent allowing the use of their blood for research
376 purposes. Peripheral blood mononuclear cells (PBMC) were separated using Ficoll-Paque (GE
377 Healthcare), and monocytes were isolated by positive selection using CD14+ magnetic beads (Miltenyi
378 Biotec) and differentiated into macrophages for 7 days in RPMI (Gibco, Life Technologies)
379 supplemented with 5% fetal calf serum (FCS; Gibco), 5% human serum AB (Sigma), penicillin-
380 streptomycin (Gibco), and 25 ng/ml macrophage colony-stimulating factor (M-CSF; Miltenyi Biotec).

381 HeLa and HEK 293 FT cells were maintained by bi-weekly subpassage in DMEM (Gibco, Thermofisher
382 Scientific), supplemented with FCS and antibiotics.

383

384 Virus production and monocyte transduction with LifeAct-mCherry

385 Viral particles were produced by transfection of 293FT cells in 6-well plates with 3 μg of total DNA and
386 8 mL TransIT-293 Transfection Reagent (Mirus Bio) per well. Plasmid mixes to produce HIV-1 viral
387 particles consisted of 0.4 μg CMV-VSVG (pMD2.G; 12259; Addgene) and 2.6 μg of HIV proviral plasmid.
388 To quantify viral release we preferentially used viral particles produced from pNL-ΔENV-VSVG which
389 was kindly provided by O. Schwartz (Institut Pasteur, Paris, France). For examination of the VCC by
390 microscopy we employed the pNL-GAG-iGFP-ΔENV-VSVG, a viral construct in which EGFP is placed
391 between viral protease cleaving sites and between the matrix and capsid domains of Gag (Hubner et
392 al., 2007). Media was renewed 16 hours later, and viruses were harvested at around 48 hours after
393 transfection, filtered through a 0.45 μm pore and stored at -80°C until use. Thawed viral stocks were
394 titrated by infecting the GHOST X4R5 reporter cell line.

395 A similar protocol was followed to produce lentiviral particles for monocyte transduction with Lifeact
396 m-cherry. Here, transfection mixes consisted of 0.4 μg CMV-VSVG, 1.0 μg of the packaging plasmid
397 PSPAX2 (12260; Addgene) and 1.6 μg of LifeAct-mCherry lentivector (pCDH1-CMV-LifeAct-mCherry).
398 In parallel, VPX-containing SIV particles were produced by transfecting 293FT cells with 0.4 μg CMV-
399 VSVG and 2.6 μg of pSIV3^{+} plasmid (Mangeot et al., 2000). Monocytes were transduced with equal
400 volumes of freshly harvested LifeAct-mCherry and SIV3 lentiviral particles in the presence of 8 μg/mL
401 of protamine (Sigma). At 48 hours, differentiating MDMs were exposed to 2 μg/mL of puromycin to
402 select for successfully transduced cells, and were harvested for experiments at day 7 of differentiation.

403

404 *In vitro* infections and cell treatments

405 MDMs were infected with HIV-1 NL-GAG-iGFP-ΔENV-VSVG or NL-ΔENV-VSVG at a MOI of 1.0. After 16
406 hours, culture media was renewed, and the infection allowed to progress for further 72 hours. At day
407 4 after infection, cells were exposed to the drugs or vehicle (DMSO) at concentrations and for the time
408 periods indicated in figure legends. Jasplakinolide (Sigma); CK666 (Sigma); Blebbistatin (Sigma);
409 Mycalolide B (Enzo Life Sciences); PF431396 (Tocris).

410 HeLa cells were infected with NL-ΔENV-VSVG at a MOI=1.0. After 16 hours, the culture media was
411 renewed, and the same drugs added at similar concentrations.

412 To assess the membrane connectivity of the VCC, we employed the CellBrite Fix membrane stain.
413 Briefly, infected MDMs were rinsed in PBS and incubated for 15 min at 37°C with a 1/1000 dilution of
414 CellBrite Fix-640 (Biotium). Cells were rinsed twice with PBS and fixed in PFA 4% for confocal
415 microscopy.

416 To assess the accessibility of VCC to anti-CD44 antibodies, infected MDMs were rinsed in PBS and
417 stained with anti-CD44 antibodies at RT for 15 mins, before rinsing twice with PBS and fixation with
418 PFA 4%. Cells were subsequently processed for confocal microscopy as described below.

419

420 Macrophage Micropatterning

421 We employed a deep UV light-based method to imprint micropatterns onto glass coverslips. 12-mm
422 coverslips were plasma treated and incubated with a solution of 0.1 mg/mL of poly(acrylamide)- g -
423 (PEG, 1,6-hexanediamine,3-aminopropyldimethylethoxysilane, (PAcrAm-g-(PEG, NH2, Si), Surface
424 Solutions, Zurich) (Serrano et al., 2016) in 10 mM HEPES pH=7.4. A quartz mask containing the
425 transparent motives for micropatterning was thoroughly washed with 70% ethanol, and coverslips
426 were attached to its quartz surface using a small volume of water. The mask was then subjected to
427 deep UV illumination in an UV ozone oven (UVO cleaner, model 342-220, Jelight) for 10 min into its
428 silver face to induce degradation of PEG chains in the coverslips accessible through the transparent
429 motives. Coverslips were finally detached from the mask and incubated for 1 hour at RT with a 5 μg/mL
430 solution of fibronectin (Sigma) in NaHCO3 100 mM. MDMs, previously infected with HIV-1 NL-GAG-
431 iGFP-ΔENV-VSVG (MOI=1.0) for 3 days, were seeded over patterned coverslips (20000 cells per
432 coverslip) in pre-warmed media and allowed to attach for 1 hour at 37°C. Non-adherent cells were
433 washed by media changes and the adherent cells were fixed in PFA 4%.

434

435 Frustrated Phagocytosis

436 Twelve mm glass coverslips were extensively washed with 70% ethanol, dried and incubated with 10
437 μg/mL of IgG from human serum (Sigma) in PBS for 1 hour at RT. For quantification of p24 release, 24-
438 well culture plates were directly coated with human IgG. MDM were infected with HIV-1 NL-GAG-
439 iGFP-ΔENV-VSVG for microscopy, or with HIV-1 NL-ΔENV-VSVG for p24 quantification at a MOI=1.0.
440 At day 3 after infection, cells were detached, washed and seeded over IgG-coated substrates (5000
441 cells for microscopy, 20000 for p24 quantification). Cells were subsequently fixed in PFA at 30 mins
442 for fixed cell confocal microscopy, or immediately imaged for live cell imaging. For p24 release
443 quantification, aliquots of the supernatant were collected at the indicated time-points, filtered
444 (0.45μm) to remove floating cells, and stored until quantification by the p24 CBA.

445

446 Quantification of p24 in culture supernatant or cell lysates by cytometric bead array (CBA)

447 Culture supernatant or cell pellets were lysed in a buffer containing 0.1% BSA, 1% NP-40 and 0.02%
448 Tween-20. The amount of p24 in samples was subsequently quantified by a custom-made CBA assay
449 that detects the HIV-1 p24 protein. Briefly, B6 functional beads (BD Biosciences) were conjugated with
450 an anti-GAG antibody (H183-H12-5C hybridoma (mouse IgG1), NIH) and serve as capturing beads by
451 incubation with samples for 1 hour at room temperature with agitation. An anti-p24 detection
452 antibody (KC57-FITC, Beckmann Coulter) is subsequently added and incubated for 2 hours at RT. After
453 two washes in a buffer containing 0.1% NP-40, beads are flowed in a FACS Verse (BD Biosciences) and
454 the p24 concentration in culture estimated using a standard curve with serial dilutions of recombinant
455 p24. For cell lysates an aliquot of the sample was used to quantify total protein by the BCA method
456 (Pierce Micro BCA kit, Thermo Fisher Scientific) and the data is presented as μg of p24 / mg of total
457 cell protein.

458

459 Western Blot

460 Cells were lysed in RIPA buffer and total protein levels quantified with the BCA method. 30 μg of
461 sample was reduced with Laemmli buffer, boiled and loaded in pre-cast polyacrylamide gels (BioRad).
462 After transfer onto PDVF membranes (BioRad), blocking buffer (5% non-fat dry milk (m/v) in PBS-
463 Tween-20 0.1% (v/v)) was added for 1 hour at RT. Primary antibodies were added overnight at 4°C
464 with gentle agitation in antibody dilution buffer (5% BSA in PBST), washed and incubated with species-
465 matched secondary HRP-conjugated secondary antibodies for 1 hour at RT. Membranes were revealed

466 in a BioRad Chemidoc after addition of HRP substrate (Clarity, Biorad). Densitometry quantifications
467 were performed using the ImageLab software (BioRad).

468

469 Confocal microscopy and Immunostaining

470 Cells were fixed in 4% paraformaldehyde (PFA), washed in PBS and then permeabilized with
471 permeabilization buffer (BSA 1% (m/v), Triton X-100 0.3% (v/v) in PBS) for 1 hour at room temperature.
472 The primary antibodies used were anti-F-actin, anti-CD18, anti-pPYK2 and anti-CD44, as listed in
473 supplementary table 1. Primary antibodies were diluted in permeabilization buffer, and the staining
474 was performed overnight at 4°C in the dark. Subsequently, cells were washed 3 times and secondary
475 staining was done in permeabilization buffer supplemented with 5% Donkey serum (Sigma) for 1 hour.
476 For secondary antibodies, donkey anti-rabbit A647 or donkey anti-mouse Alexa 647 (Invitrogen) were
477 used. Phalloidin-AF647 (Invitrogen) staining was also performed at this stage. Cells were washed 3
478 times then rinsed in PBS and mounted in Fluoromont-GTM medium with DAPI (Invitrogen).

479 Cell imaging was performed on an inverted confocal microscope (Leica DMi8, SP8 scanning head unit)
480 equipped with a 63x oil immersion objective (NA=1.4) and four laser diodes (405, 488, 546, and 633
481 nm). An optimized z-step of 0.31 μm was employed.

482

483 Image analysis and quantification

484 Image J was used for all image analyses and quantifications, using custom-made macro scripts to
485 automate the analysis. The Gag-iGFP signal was used to define a binary mask on the VCC, at each z-
486 slice. The total volume of the VCC was then obtained by summation of the binary mask value, at each
487 x,y pixel, across all the z-stack, correcting for the known dimensions of the voxel. A similar strategy
488 was employed to estimate the total cell volume. Depending on the staining, the binary masks to define
489 the cell area at each z-slice were derived from the phalloidin, F-actin or CD18 staining. Mean Gag
490 intensity corresponds to the average Gag-iGFP signal at the region defined as the VCC by the binary
491 mask.

492 To calculate VCC dispersion (spreading) across the cell, we used maximum intensity projections of the
493 VCC's binary mask and determined its centroid. Spreading was then determined by calculating the
494 average distance of each VCC's pixel in the projected mask to the centroid. A similar strategy was used
495 to calculate the average distance of the VCC to the nuclear centroid. In this case, DAPI was used to
496 define the nuclear binary mask, which after maximum intensity projection, was used to determine its
497 centroid.

498 To determine the enrichment of CD18, p-PYK2 or CellBrite at the VCC, we first defined the VCC and
499 cell binary masks and obtained the average intensity for the CD18, p-PYK2 or CellBrite staining in both
500 the VCC and the whole cell. The enrichment score was then obtained as the ratio between the average
501 intensity at the VCC and the average intensity in the whole cell.

502 All image montages were assembled using ImageJ. Y-projections were obtained using the Reslice tool,
503 followed by maximum intensity projections. The 3D reconstructions which were achieved by applying
504 the Volume Viewer plugin to the binary masks of the channels imaged.

505

506 Live cell imaging

507 For live imaging experiments, cells were imaged on an inverted confocal microscope (Leica DMi8, SP8
508 scanning head unit) equipped with a 40X oil immersion objective and a live cell imaging chamber to
509 maintain a constant temperature of 37°C and CO2 levels of 5%.

510 To assess the dynamics of the actin cytoskeleton surrounding the VCC, MDMs transduced with lifeact-
511 mCherry were infected with HIV-1 GAG-iGFP ΔENV-VSVG at a MOI=1.0 for 6 days in glass bottom 35-
512 mm dishes (Ibidi). Z-stacks were acquired in real-time at a frame rate of 0.42/s.

513 To image infected MDMs during frustrated phagocytosis, cells were placed in the imaging chamber
514 immediately after their addition to IgG-coated 35-mm glass bottom disks. Z-stacks were acquired at a
515 frame rate of 0.041/s. Acquired images were processed in ImageJ to assemble videos and montages.

516

517 Electron microscopy

518 MDMs infected with HIV-1-NL-ΔENV-VSVG, were fixed in 2% glutaraldehyde in 0.1 M cacodylate
519 buffer, pH 7.4 for 1 hour and subsequently fixed for 1 hour in 2% buffered osmium tetroxide,
520 dehydrated in a graded series of ethanol solution, and then embedded in epoxy resin. Images were
521 acquired with a digital camera Quemesa (SIS) mounted on a Tecnai Spirit transmission electron
522 microscope (FEI) operated at 80 kV.

523

524 Statistical analysis

525 Data were analysed using Prism software v9 (GraphPad). If not specified in figure legends, graphics
526 show individual donors as dots with bars or lines at the means. Distributions were assumed to be non-
527 parametric, and the specific test employed is indicated at the figure legend. ns, P value of >0.05; *, P
528 value of ≤0.05; **, P value of ≤0.01; ***, P value of ≤0.001; ****, P value of ≤0.0001.

Acknowledgements

We thank Dr Claire Hivroz and Ana-Maria Lennon-Dumenil at Institut Curie for fruitful discussions and critical reading of the manuscript. We also thank François-Xavier Gobert and Nicolas Carpi for discussions or technical help. This work was supported by grants from Agence Nationale de Recherche contre le SIDA et les hépatites virales (ANRS), Ensemble contre le SIDA (Sidaction), Laboratoire d'Excellence (Labex) DCBIOL (ANR-10-IDEX-0001-02 PSL and ANR-11-LABX-0043) to P.B. V.R. was supported by fellowships from ANRS and Sidaction.

Author Contributions

VR and PB designed the research. VR, ST, MSR, EG and AH performed the research. MM wrote the scripts for image analysis. VR, ST and MSR analysed the data. VR and PB supervised research. VR, ST and PB wrote the paper.

542 **Figure Legends**

543

544 **Figure 1.** Actin is involved in VCC dynamics and viral release from macrophages

545 **A** – MDM infected with HIV-1 GAG-iGFP-ΔENV-VSVG for 7 days, stained for phalloidin. Scale bar = 30
546 µm. The bottom panel shows a maximum intensity z-projection. The top panel shows a slice on the xz
547 plane, highlighting the selected region for panel 1B.

548 **B** – Maximum intensity Z projection and 3D volume rendering of the region highlighted in 1A. Scale
549 bar = 1 µm

550 **C** – MDMs transduced with Lifeact-mCherry were infected with HIV-1-GAG-iGFP-dENV-VSVG
551 (MOI=1.0). Time-lapse imaging was performed at day 6 after infection. The bottom panels represent
552 the dashed region in the top panels. Scale bar= 20um (top panels) and 5um (bottom panels)

553 **D** – MDMs were infected with HIV-1-ΔENV-VSVG at a MOI=1.0 for 4 days. Cells were subsequently
554 treated with the indicated drugs for 24 hours. Supernatant aliquots were recovered at the indicated
555 time-points, and the released p24 was quantified by a custom-made CBA assay. Jasplakinolide = 50
556 nM / CK666 = 10 µM / Blebbistatin = 5 µM / Mycalolide-B = 100 nM. Data from 3 independent donors.
557 Two-way ANOVA. *= P<0.05

558 **E** – As in (D), cells were lysed at the end of the experimental procedure in NP-40 lysis buffer and
559 intracellular p24 was quantified by CBA. Data from 3 independent donors. One-Way ANOVA – (** =
560 P<0.01; *** P<0.001).

561 **F** – As in (D), cells were lysed in RIPA buffer at the end of the experimental procedure and analysed by
562 western blot for the expression of GAG. One representative donor is shown.

563 **G** – Densitometry quantification of the western blot bands from (F) for 3 independent donors. Paired
564 t-test, * = P<0.05, ns- non-significant

565

566 **Figure 2**. Stabilization of actin fibres scatters the VCC and increases the total volume of the
567 compartment

568 **A** – MDMs were grown in coverslips, infected with HIV-1-ΔENV-GAG-iGFP-VSVG at a MOI=1.0 for 4
569 days and subsequently treated with DMSO or jasplakinolide (100 nM) for 24 hours. Cells were fixed,
570 stained with anti-F-actin and imaged by confocal microscopy.

571 **B-F** – Image analysis for cells processed as in (E) for the indicated parameters. See methods for details
572 on the quantification strategies employed. Each circle represents one cell and the plots display cells
573 from 3 independent donors. Unpaired t-test. (** = $P<0.01$; ****$P<0.0001$).

574 **G** – Cells were treated as in (A) and processed for electron microscopy. The right panels are
575 enlargements of the areas enclosed in the dashed squares on the left panels. Scale bar = 2 µm (left
576 panels), 1 µm (right panel).

577

578 **Figure 3**. Stabilization of actin fibres relocalizes the integrin CD18 away from the VCC limiting
579 membrane in HIV-1-infected macrophages

580 **A-B** – MDMs were infected HIV-1-ΔENV-VSVG (MOI=1.0) for 7 days. Cells were fixed and processed
581 for electron microscopy. (A) depicts an example of an internal VCC with associated electron dense
582 coats. (B) highlights the presence of compartments with coats close to the cell surface. Arrow heads
583 point to the electron dense coats. Scaler bars= 2 µm.

584 **C** – Confocal microscopy of MDMs infected with HIV-1-Gag-iGFP-ΔENV-VSVG (MOI=1.0) for 4 days and
585 treated with jasplakinolide or DMSO for 24 hours. Whole cell projections are shown in the right, along
586 the z-axis (bottom) or the y axis (top). On the left, the areas enclosed in the dashed squares are
587 enlarged and shown as z-projections. Scale bar = 20 µm (left panels) or 2 µm (right panels).

588 **D** – Quantification of CD18 enrichment at the VCC by image analysis. Each dot represents a single cell
589 from 3 independent donors. See Methods for details on the analysis.

590 **E** – **F** - Electron microscopy of MDMs infected with HIV-1-ΔENV-VSVG (MOI=1.0) for 4 days and treated
591 with jasplakinolide or DMSO for 24 hours. Arrow heads point to electron dense regions associated
592 with the VCC in DMSO treated cells (note their absence in cells treated with jasplakinolide). Scale bars=
593 2 µm.

594

595 **Figure 4**. The phosphorylated form of integrin-associated kinase PYK2 partially colocalizes with the
596 VCC

597 **A** – MDMs left uninfected or infected with HIV-1-Δ-ENV-VSVG (MOI=1.0) for 4 days were treated with
598 jasplakinolide or vehicle (DMSO) for 24 hours. Cells were lysed and analysed by western blot for the
599 indicated proteins. The higher concentration of Jasplakinolide employed was 200 nM and the lower
600 concentrations correspond to consecutive two-fold dilutions.

601 **B** – Confocal microscopy of MDMs infected with HIV-1-Gag-iGFP-ΔENV-VSVG (MOI=1.0) for 4 days and
602 treated with jasplakinolide or DMSO for 24 hours. Whole cell projections are shown on the right, along
603 the z-axis (bottom) or the y axis (top). On the left, the areas enclosed in the dashed squares are
604 enlarged and shown as z-projections. Scale bar = 20 µm (left panels) or 2 µm (right panels).

605 **C** – Quantification of P-(Y402)-PYK2 enrichment at the VCC by image analysis. Each dot represents a
606 single cell from 2 independent donors. See Methods for details on the analysis.

607

608 **Figure 5**. A PYK2 inhibitor promotes HIV-1 retention in VCC

609 **A** – MDMs left uninfected or infected with HIV-1-Δ-ENV-VSVG (MOI=1.0) for 4 days were treated with
610 PF396 or vehicle (DMSO) for additional 96 hours. Cells were lysed and analysed by western blot with
611 the indicated antibodies. The table below the blots display the intensity ratios indicated, as measured
612 by densitometry.

613 **B** – MDMs were infected with HIV-1-ΔENV-VSVG at a MOI=1.0 for 4 days. Cells were subsequently
614 treated with PF396 (1µM). At the indicated time-points, supernatant aliquots were recovered, and the
615 released p24 was quantified by CBA. Data from 3 independent donors. Two-way ANOVA. *= $P<0.05$

616 **C** – As in (B), cells were lysed at the end of the experimental procedure in NP-40 lysis buffer and
617 intracellular p24 was quantified by CBA. Data from 3 independent donors. Paired t test – (** = $P<0.01$).

618 **D** – Confocal microscopy of MDMs infected with HIV-1-Gag-iGFP-ΔENV-VSVG (MOI=1.0) for 4 days and
619 treated with PF396 (1µM) or vehicle (DMSO) for an additional 96 hours. Whole cell projections are
620 shown on the right, along the z-axis (bottom) or the y axis (top). On the left, the areas enclosed in the
621 dashed squares are zoomed in and shown as z-projections. Scale bar = 20 µm (left panels) or 2 µm
622 (right panels).

623 **E-I** – Image analysis for cells processed as in (D) for the indicated parameters. See methods for details
624 on the quantification strategies employed. Each circle represents one cell, and the plots show cells
625 from 3 independent donors. Unpaired t-test. (* = $P<0.05$; *** $P<0.001$).

626 **J -** CD18 enrichment at the VCC for cells processed as in Fig. S4. See methods for details on image
627 analysis. Each circle represents one cell, and the plots display cells from 2 independent donors.
628 Unpaired t-test. (ns= not significant).

629 **K** – Confocal microscopy of MDMs infected with HIV-1-Gag-iGFP-ΔENV-VSVG (MOI=1.0) for 4 days and
630 treated with PF396 (1µM) or vehicle (DMSO) for additional 96 hours. Cells were exposed to CellBrite
631 before fixation. Right panel - whole cell projections along the z-axis (bottom) or the y axis (top). Left,

632 panels – magnification of the areas enclosed in the dashed squares as z-projections. Scale bar = 20 µm
633 (left panels) or 2 µm (right panels).

634 **L-M** – Quantification of CellBrite intensity in the VCC (L) or elsewhere in the cell (M) for cells processed
635 as in (K). See methods for details. Each circle represents one cell, and the plots show cells from 2
636 independent donors. Unpaired t-test. (Ns-non-significant; *** *P*<0.001).

637

638 **Figure 6**. Rapid HIV release during macrophage frustrated phagocytosis is associated with trafficking
639 of $CD18^+$ VCC to the surface

640 **A** – Time-lapse imaging of MDMs infected with HIV-1-GAG-iGFP-ΔENV-VSVG for 3 days and seeded
641 over human IgG-coats coverslips. Whole cell projections are shown for the top and middle panels,
642 along the z-axis (middle) or the y axis (top). The bottom panel (transmission channel) is a single z-slice.
643 Scale bar = 20 µm.

644 **B** – Image analysis of the total VCC volume (left y-axis) and the cell projected area (right y-axis) over
645 the course of the frustrated phagocytosis event depicted in (A).

646 **C** – MDMs infected with HIV-1-ΔENV-VSVG for 3 days were seeded over human IgG-coated coverslips,
647 or over non-coated coverslips, or in the presence of soluble IgG over non-coated coverslips. At the
648 indicated time-points, aliquots of the supernatant were recovered and the released p24 was
649 quantified by CBA. Data from 3 independent donors. For each time-point groups were compared by
650 one-way ANOVA (* = *P*<0.05).

651 **D** – Confocal microscopy of MDMs infected with HIV-1-Gag-iGFP-ΔENV-VSVG (MOI=1.0) for 3 days and
652 seeded over control or human IgG-coated coverslips for 30 mins. Right panels - whole cell projections
653 along the z-axis (bottom) or the y axis (top). Left, panels – magnification of the areas enclosed in the
654 dashed squares as z-projections. Scale bar = 20 µm (left panels) or 2 µm (right panels).

655 **E-H** – Image analysis for cells processed as in (D) for the indicated parameters. See methods for details
656 on the quantification strategies employed. Each circle represents one cell, and the plots include cells
657 from 2 independent donors. Unpaired t-test. (** = *P*<0.01; ****P<0.0001).

658

659 **References**

660 Bear, J.E., and Haugh, J.M. (2014). Directed migration of mesenchymal cells: where signaling
661 and the cytoskeleton meet. Curr Opin Cell Biol *30*, 74-82. 10.1016/j.ceb.2014.06.005.
662 Berre, S., Gaudin, R., Cunha de Alencar, B., Desdouits, M., Chabaud, M., Naffakh, N., Rabaza-
663 Gairi, M., Gobert, F.X., Jouve, M., and Benaroch, P. (2013). CD36-specific antibodies block
664 release of HIV-1 from infected primary macrophages and its transmission to T cells. J Exp Med
665 *210*, 2523-2538. 10.1084/jem.20130566.
666 Chalut, K.J., and Paluch, E.K. (2016). The Actin Cortex: A Bridge between Cell Shape and
667 Function. Dev Cell *38*, 571-573. 10.1016/j.devcel.2016.09.011.
668 Chu, H., Wang, J.J., Qi, M., Yoon, J.J., Wen, X., Chen, X., Ding, L., and Spearman, P. (2012). The
669 intracellular virus-containing compartments in primary human macrophages are largely
670 inaccessible to antibodies and small molecules. PLoS One *7*, e35297.
671 10.1371/journal.pone.0035297.
672 Davis, C.B., Dikic, I., Unutmaz, D., Hill, C.M., Arthos, J., Siani, M.A., Thompson, D.A.,
673 Schlessinger, J., and Littman, D.R. (1997). Signal transduction due to HIV-1 envelope
674 interactions with chemokine receptors CXCR4 or CCR5. J Exp Med *186*, 1793-1798.
675 10.1084/jem.186.10.1793.
676 Del Corno, M., Liu, Q.H., Schols, D., de Clercq, E., Gessani, S., Freedman, B.D., and Collman,
677 R.G. (2001). HIV-1 gp120 and chemokine activation of Pyk2 and mitogen-activated protein
678 kinases in primary macrophages mediated by calcium-dependent, pertussis toxin-insensitive
679 chemokine receptor signaling. Blood *98*, 2909-2916. 10.1182/blood.v98.10.2909.
680 Deneka, M., Pelchen-Matthews, A., Byland, R., Ruiz-Mateos, E., and Marsh, M. (2007). In
681 macrophages, HIV-1 assembles into an intracellular plasma membrane domain containing the
682 tetraspanins CD81, CD9, and CD53. J Cell Biol *177*, 329-341. 10.1083/jcb.200609050.
683 Duncan, C.J., Williams, J.P., Schiffner, T., Gartner, K., Ochsenbauer, C., Kappes, J., Russell, R.A.,
684 Frater, J., and Sattentau, Q.J. (2014). High-multiplicity HIV-1 infection and neutralizing
685 antibody evasion mediated by the macrophage-T cell virological synapse. J Virol *88*, 2025-
686 2034. 10.1128/JVI.03245-13.
687 Duong, L.T., and Rodan, G.A. (2000). PYK2 is an adhesion kinase in macrophages, localized in
688 podosomes and activated by beta(2)-integrin ligation. Cell Motil Cytoskeleton *47*, 174-188.
689 10.1002/1097-0169(200011)47:3<174::AID-CM2>3.0.CO;2-N.

690 Gaudin, R., Berre, S., Cunha de Alencar, B., Decalf, J., Schindler, M., Gobert, F.X., Jouve, M.,
691 and Benaroch, P. (2013). Dynamics of HIV-containing compartments in macrophages reveal
692 sequestration of virions and transient surface connections. PLoS One *8*, e69450.
693 10.1371/journal.pone.0069450.
694 Gaudin, R., de Alencar, B.C., Jouve, M., Berre, S., Le Bouder, E., Schindler, M., Varthaman, A.,
695 Gobert, F.X., and Benaroch, P. (2012). Critical role for the kinesin KIF3A in the HIV life cycle in
696 primary human macrophages. J Cell Biol *199*, 467-479. 10.1083/jcb.201201144.
697 Gousset, K., Ablan, S.D., Coren, L.V., Ono, A., Soheilian, F., Nagashima, K., Ott, D.E., and Freed,
698 E.O. (2008). Real-time visualization of HIV-1 GAG trafficking in infected macrophages. PLoS
699 Pathog *4*, e1000015. 10.1371/journal.ppat.1000015.
700 Graziano, F., Desdouits, M., Garzetti, L., Podini, P., Alfano, M., Rubartelli, A., Furlan, R.,
701 Benaroch, P., and Poli, G. (2015). Extracellular ATP induces the rapid release of HIV-1 from
702 virus containing compartments of human macrophages. Proc Natl Acad Sci U S A *112*, E3265-
703 3273. 10.1073/pnas.1500656112.
704 Hayashi-Takanaka, Y., Kina, Y., Nakamura, F., Yamazaki, S., Harata, M., Soest, R., Kimura, H.,
705 and Nakao, Y. (2019). Effect of mycalolides isolated from a marine sponge Mycale aff.
706 nullarosette on actin in living cells. Sci Rep *9*, 7540. 10.1038/s41598-019-44036-2.
707 Hubner, W., Chen, P., Del Portillo, A., Liu, Y., Gordon, R.E., and Chen, B.K. (2007). Sequence of
708 human immunodeficiency virus type 1 (HIV-1) Gag localization and oligomerization monitored
709 with live confocal imaging of a replication-competent, fluorescently tagged HIV-1. J Virol *81*,
710 12596-12607. 10.1128/JVI.01088-07.
711 Ladinsky, M.S., Khamaikawin, W., Jung, Y., Lin, S., Lam, J., An, D.S., Bjorkman, P.J., and Kieffer,
712 C. (2019). Mechanisms of virus dissemination in bone marrow of HIV-1-infected humanized
713 BLT mice. Elife *8*. 10.7554/eLife.46916.
714 Mangeot, P.E., Negre, D., Dubois, B., Winter, A.J., Leissner, P., Mehtali, M., Kaiserlian, D.,
715 Cosset, F.L., and Darlix, J.L. (2000). Development of minimal lentivirus vectors derived from
716 simian immunodeficiency virus (SIVmac251) and their use for gene transfer into human
717 dendritic cells. J Virol *74*, 8307-8315. 10.1128/jvi.74.18.8307-8315.2000.
718 Masters, T.A., Pontes, B., Viasnoff, V., Li, Y., and Gauthier, N.C. (2013). Plasma membrane
719 tension orchestrates membrane trafficking, cytoskeletal remodeling, and biochemical
720 signaling during phagocytosis. Proc Natl Acad Sci U S A *110*, 11875-11880.
721 10.1073/pnas.1301766110.

722 Mlcochova, P., Pelchen-Matthews, A., and Marsh, M. (2013). Organization and regulation of
723 intracellular plasma membrane-connected HIV-1 assembly compartments in macrophages.
724 BMC Biol *11*, 89. 10.1186/1741-7007-11-89.
725 Okigaki, M., Davis, C., Falasca, M., Harroch, S., Felsenfeld, D.P., Sheetz, M.P., and Schlessinger,
726 J. (2003). Pyk2 regulates multiple signaling events crucial for macrophage morphology and
727 migration. Proc Natl Acad Sci U S A *100*, 10740-10745. 10.1073/pnas.1834348100.
728 Olazabal, I.M., Caron, E., May, R.C., Schilling, K., Knecht, D.A., and Machesky, L.M. (2002). Rho-
729 kinase and myosin-II control phagocytic cup formation during CR, but not FcgammaR,
730 phagocytosis. Curr Biol *12*, 1413-1418. 10.1016/s0960-9822(02)01069-2.
731 Orenstein, J.M., Meltzer, M.S., Phipps, T., and Gendelman, H.E. (1988). Cytoplasmic assembly
732 and accumulation of human immunodeficiency virus types 1 and 2 in recombinant human
733 colony-stimulating factor-1-treated human monocytes: an ultrastructural study. J Virol *62*,
734 2578-2586. 10.1128/JVI.62.8.2578-2586.1988.
735 Ospina Stella, A., and Turville, S. (2018). All-Round Manipulation of the Actin Cytoskeleton by
736 HIV. Viruses *10*. 10.3390/v10020063.
737 Pelchen-Matthews, A., Giese, S., Mlcochova, P., Turner, J., and Marsh, M. (2012). beta2
738 integrin adhesion complexes maintain the integrity of HIV-1 assembly compartments in
739 primary macrophages. Traffic *13*, 273-291. 10.1111/j.1600-0854.2011.01306.x.
740 Rahman, S.A., Koch, P., Weichsel, J., Godinez, W.J., Schwarz, U., Rohr, K., Lamb, D.C.,
741 Krausslich, H.G., and Muller, B. (2014). Investigating the role of F-actin in human
742 immunodeficiency virus assembly by live-cell microscopy. J Virol *88*, 7904-7914.
743 10.1128/JVI.00431-14.
744 Rodrigues, V., Ruffin, N., San-Roman, M., and Benaroch, P. (2017). Myeloid Cell Interaction
745 with HIV: A Complex Relationship. Front Immunol *8*, 1698. 10.3389/fimmu.2017.01698.
746 Sattentau, Q.J., and Stevenson, M. (2016). Macrophages and HIV-1: An Unhealthy
747 Constellation. Cell Host Microbe *19*, 304-310. 10.1016/j.chom.2016.02.013.
748 Schaller, M.D. (2010). Cellular functions of FAK kinases: insight into molecular mechanisms
749 and novel functions. J Cell Sci *123*, 1007-1013. 10.1242/jcs.045112.
750 Serrano, A., Zurcher, S., Tosatti, S., and Spencer, N.D. (2016). Imparting Nonfouling Properties
751 to Chemically Distinct Surfaces with a Single Adsorbing Polymer: A Multimodal Binding
752 Approach. Macromol Rapid Commun *37*, 622-629. 10.1002/marc.201500683.

753 Thery, M. (2010). Micropatterning as a tool to decipher cell morphogenesis and functions. J
754 Cell Sci *123*, 4201-4213. 10.1242/jcs.075150.
755 Thomas, A., Mariani-Floderer, C., Lopez-Huertas, M.R., Gros, N., Hamard-Peron, E., Favard, C.,
756 Ohlmann, T., Alcami, J., and Muriaux, D. (2015). Involvement of the Rac1-IRSp53-Wave2-
757 Arp2/3 Signaling Pathway in HIV-1 Gag Particle Release in CD4 T Cells. J Virol *89*, 8162-8181.
758 10.1128/JVI.00469-15.
759 Van Goethem, E., Poincloux, R., Gauffre, F., Maridonneau-Parini, I., and Le Cabec, V. (2010).
760 Matrix architecture dictates three-dimensional migration modes of human macrophages:
761 differential involvement of proteases and podosome-like structures. J Immunol *184*, 1049-
762 1061. 10.4049/jimmunol.0902223.
763 Verollet, C., Souriant, S., Bonnaud, E., Jolicoeur, P., Raynaud-Messina, B., Kinnaer, C.,
764 Fourquaux, I., Imle, A., Benichou, S., Fackler, O.T., et al. (2015). HIV-1 reprograms the
765 migration of macrophages. Blood *125*, 1611-1622. 10.1182/blood-2014-08-596775.
766 Welsch, S., Keppler, O.T., Habermann, A., Allespach, I., Krijnse-Locker, J., and Krausslich, H.G.
767 (2007). HIV-1 buds predominantly at the plasma membrane of primary human macrophages.
768 PLoS Pathog *3*, e36. 10.1371/journal.ppat.0030036.
769 Wen, X., Ding, L., Wang, J.J., Qi, M., Hammonds, J., Chu, H., Chen, X., Hunter, E., and
770 Spearman, P. (2014). ROCK1 and LIM kinase modulate retrovirus particle release and cell-cell
771 transmission events. J Virol *88*, 6906-6921. 10.1128/JVI.00023-14.
772 Zhu, X., Bao, Y., Guo, Y., and Yang, W. (2018). Proline-Rich Protein Tyrosine Kinase 2 in
773 Inflammation and Cancer. Cancers (Basel) *10*. 10.3390/cancers10050139.
774
775

Figure 1.

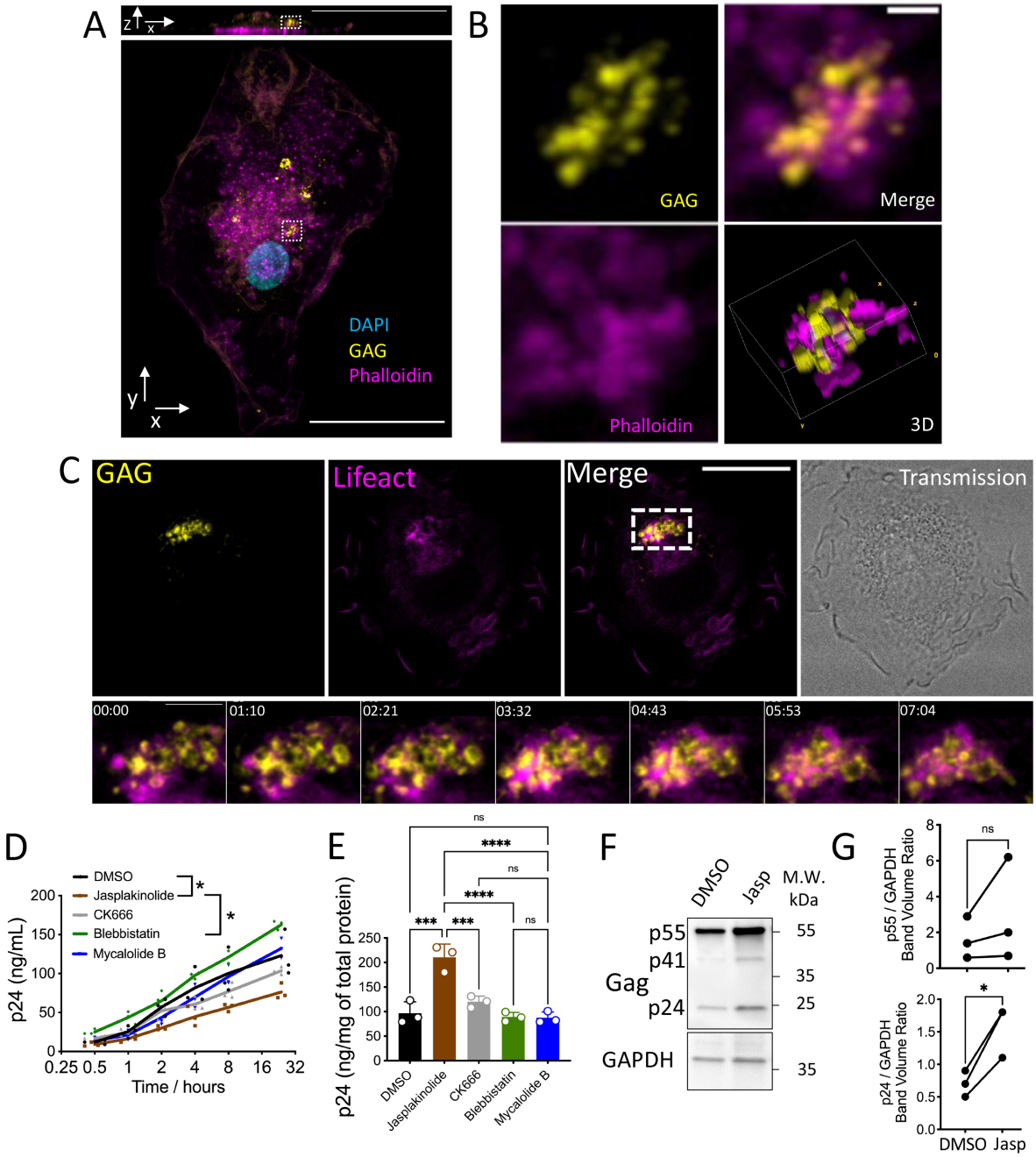
A
z
x
DAPI
GAG
Phalloidin
y
x
B
GAG
Merge
Phalloidin
3D
C
GAG
Lifeact
Merge
Transmission
00:00
01:10
02:21
03:32
04:43
05:53
07:04
D
DMSO
Jasplakinolide
CK666
Blebbistatin
Mycalolide B
p24 (ng/mL)
Time / hours
E
p24 (ng/mg of total protein)
DMSO
Jasplakinolide
CK666
Blebbistatin
Mycalolide B
F
DMSO
Jasp
M.W. kDa
p55
p41
Gag
p24
GAPDH
55
35
25
35
G
p55 / GAPDH Band Volume Ratio
p24 / GAPDH Band Volume Ratio
DMSO
Jasp

779 **Figure 2.**

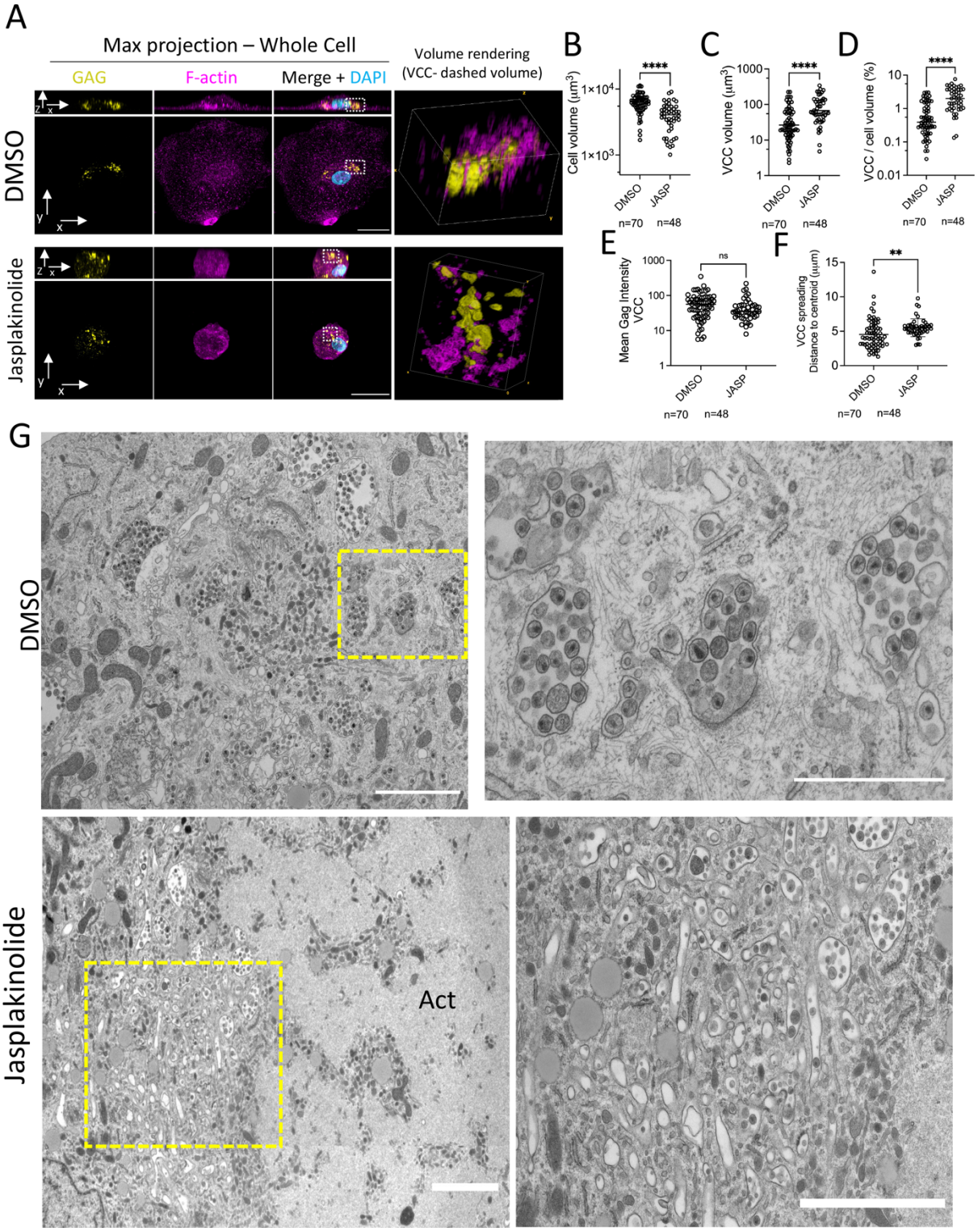

780

781

782

783 **Figure 3.**

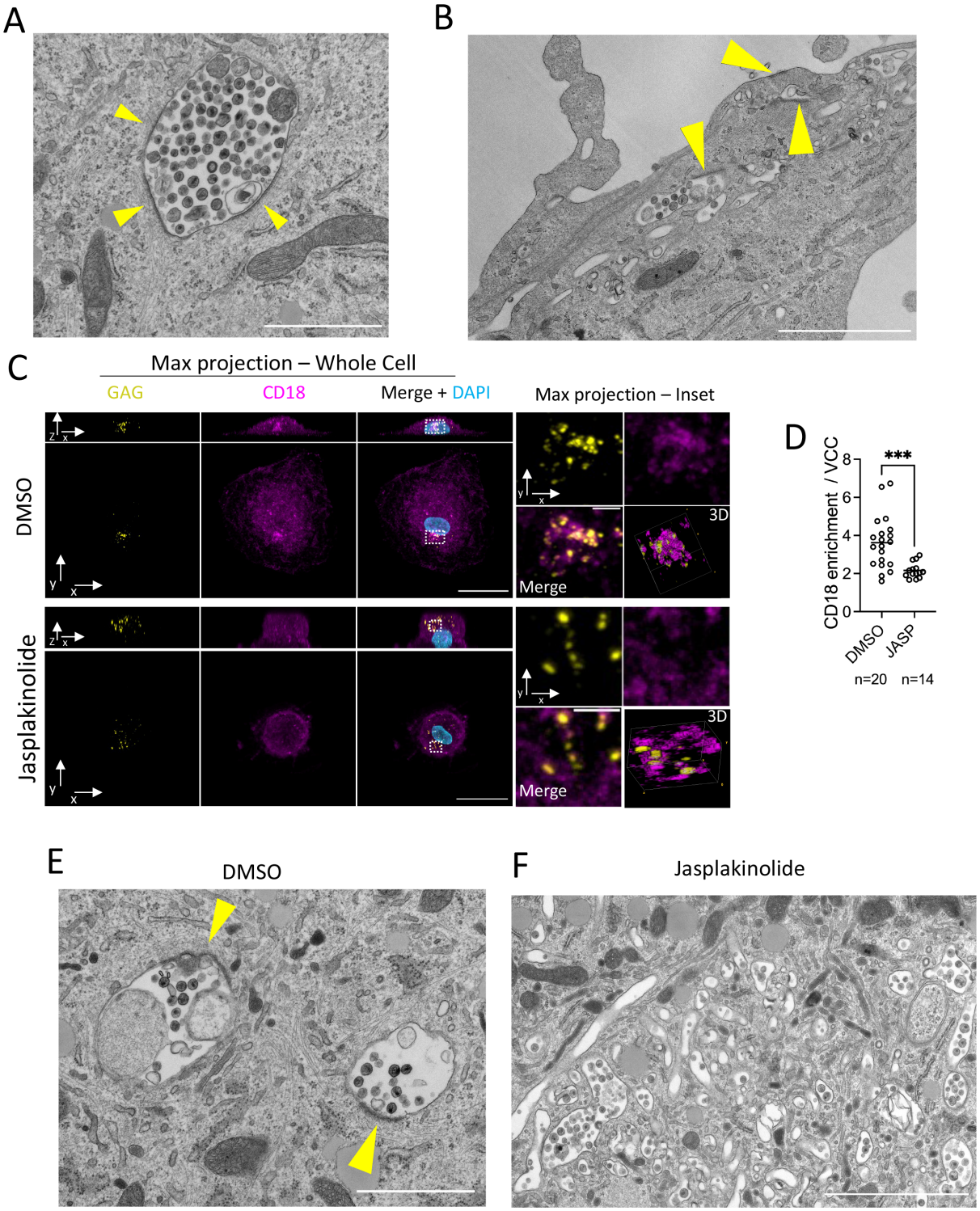

784

785

786

787

788

Figure 4.

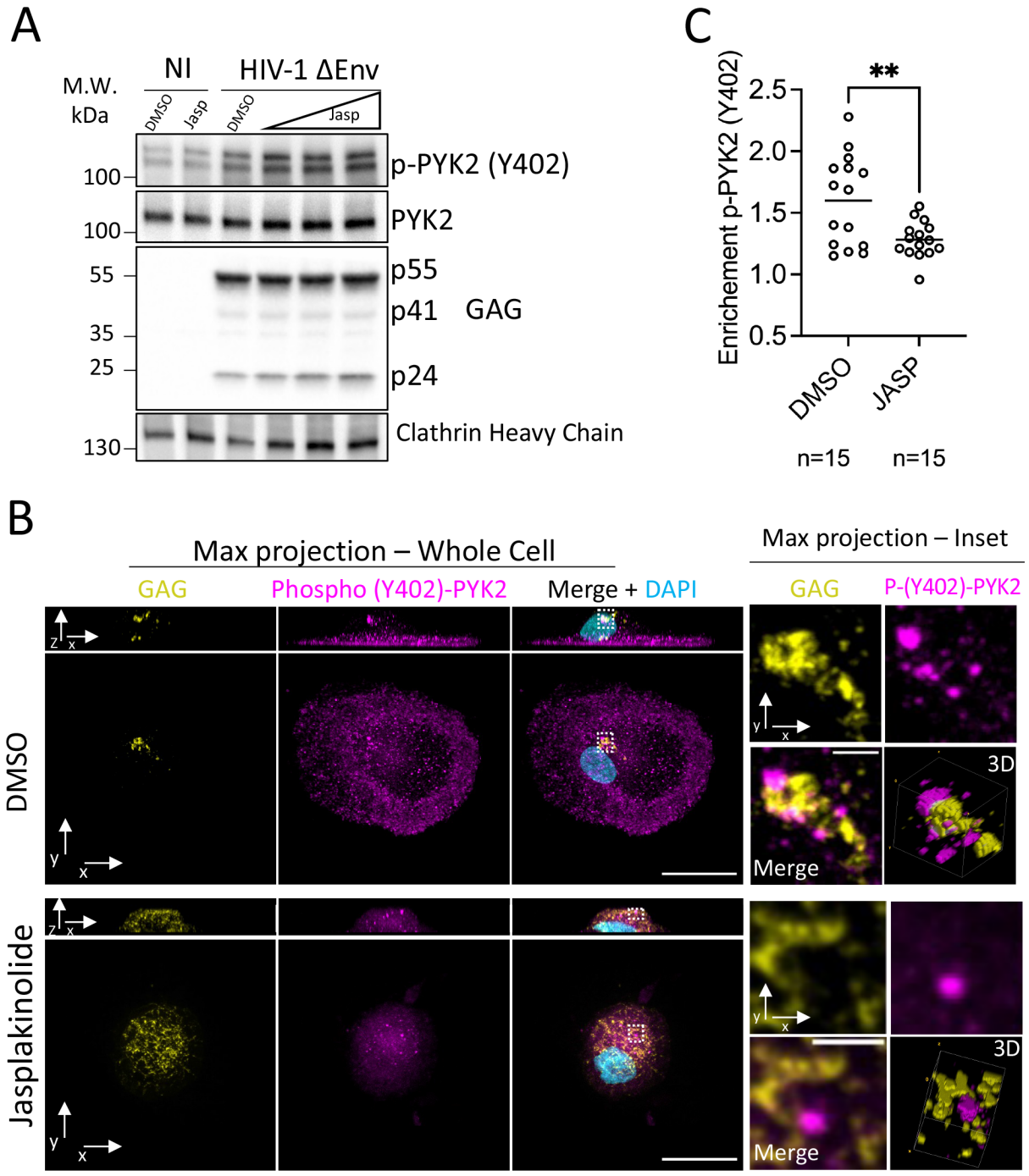
A
M.W.
kDa
NI
HIV-1 ΔEnv
DMSO
Jasp
DMSO
Jasp
100
100
55
35
25
130
p-PYK2 (Y402)
PYK2
p55
p41
GAG
p24
Clathrin Heavy Chain
C
Enrichement p-PYK2 (Y402)
2.5
2.0
1.5
1.0
0.5
**
DMSO
JASP
n=15
n=15
B
Max projection – Whole Cell
Max projection – Inset
GAG
Phospho (Y402)-PYK2
Merge + DAPI
GAG
P-(Y402)-PYK2
DMSO
Jasplakinolide
3D
Merge
3D
Merge

Figure 5.

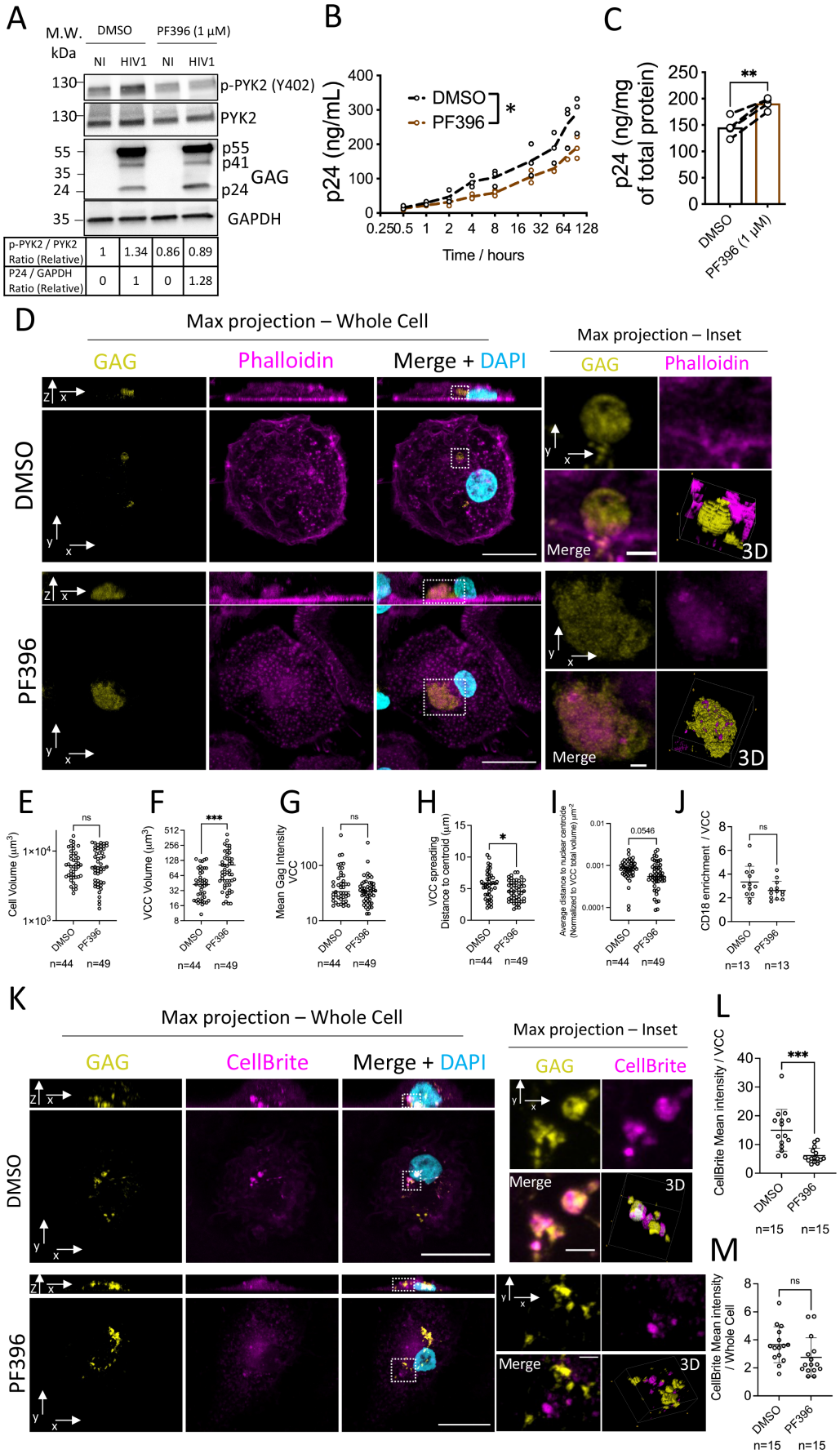
A
M.W. kDa
DMSO
PF396 (1 µM)
NI
HIV1
NI
HIV1
130
p-PYK2 (Y402)
130
PYK2
55
35
24
p55
p41
p24
GAG
35
GAPDH
p-PYK2 / PYK2 Ratio (Relative) 1 1.34 0.86 0.89
P24 / GAPDH Ratio (Relative) 0 1 0 1.28
B
p24 (ng/mL)
DMSO
PF396
*
Time / hours
C
p24 (ng/mg of total protein)
**
DMSO
PF396 (1 µM)
D
Max projection – Whole Cell
GAG
Phalloidin
Merge + DAPI
Max projection – Inset
GAG
Phalloidin
DMSO
PF396
Merge
3D
E
Cell Volume (µm³)
ns
DMSO
PF396
n=44
n=49
F
VCC Volume (µm³)
***
G
Mean Gag Intensity VCC
ns
H
VCC spreading Distance to centroid (µm)
*
I
Average distance to nuclear centroid (Normalized to VCC total volume) µm⁻²
0.0546
J
CD18 enrichment / VCC
ns
n=13
n=13
K
Max projection – Whole Cell
GAG
CellBrite
Merge + DAPI
Max projection – Inset
GAG
CellBrite
DMSO
PF396
Merge
3D
L
CellBrite Mean intensity / VCC
***
n=15
n=15
M
CellBrite Mean intensity / Whole Cell
ns
n=15
n=15

Figure 6.

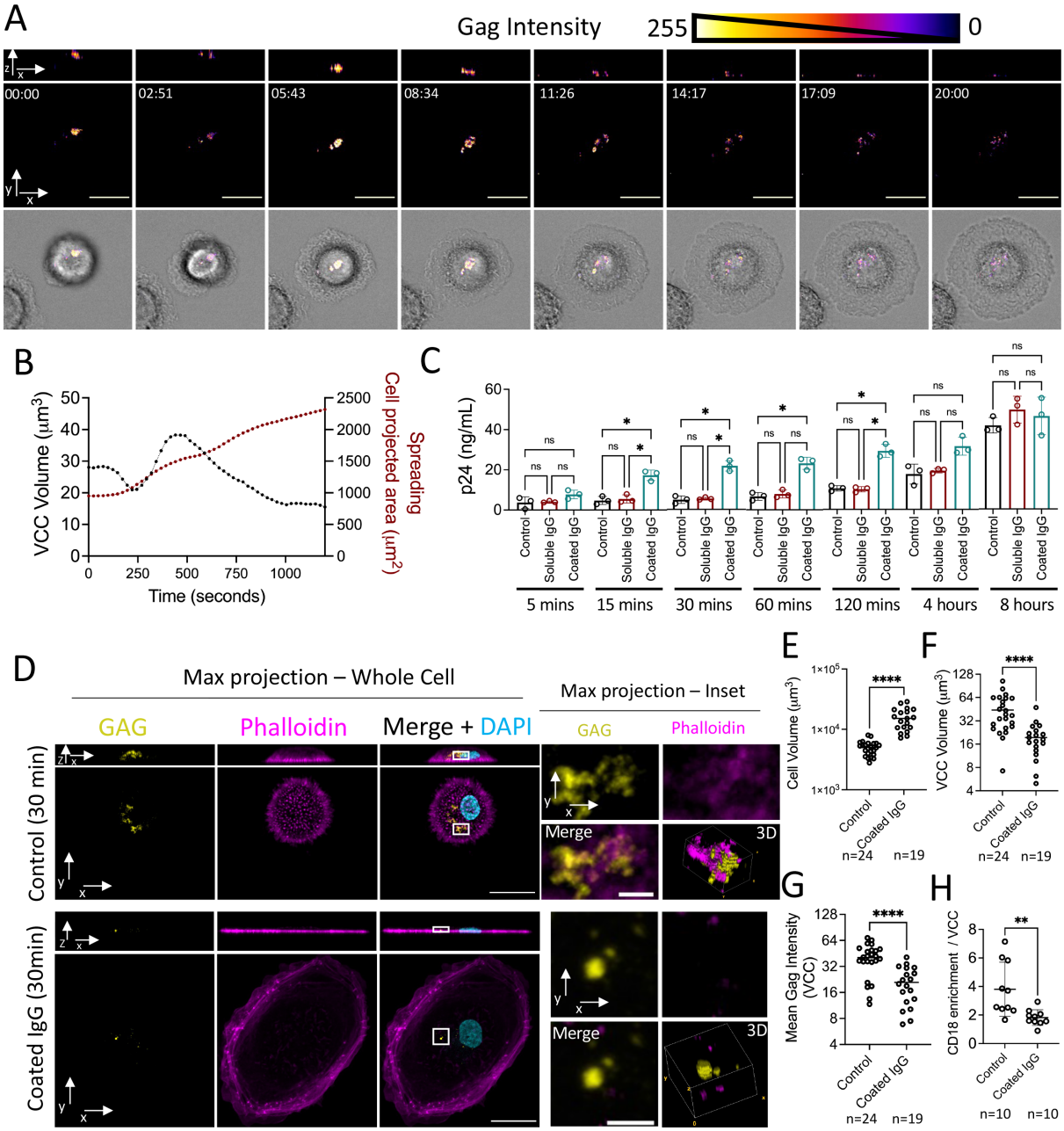
A
Gag Intensity
255
0
00:00
02:51
05:43
08:34
11:26
14:17
17:09
20:00
B
VCC Volume (µm³)
Spreading
Cell projected area (µm²)
Time (seconds)
C
p24 (ng/mL)
Control
Soluble IgG
Coated IgG
5 mins
15 mins
30 mins
60 mins
120 mins
4 hours
8 hours
D
Max projection – Whole Cell
Max projection – Inset
GAG
Phalloidin
Merge + DAPI
Control (30 min)
Coated IgG (30min)
Merge
3D
E
Cell Volume (µm³)
F
VCC Volume (µm³)
G
Mean Gag Intensity (VCC)
H
CD18 enrichment / VCC
n=24
n=19
n=10